The Astrophysical Journal, 788:191 (9pp), 2014 June 20 doi:10.1088/0004-637X/788/2/191

THEORETICAL UV ABSORPTION SPECTRA OF HYDRODYNAMICALLY ESCAPING O_2/CO_2-RICH EXOPLANETARY ATMOSPHERES

G. Gronoff[1,2], R. Maggiolo[3], C. Simon Wedlund[4], C. J. Mertens[1], R. B. Norman[1], J. Bell[5], D. Bernard[6], C. J. Parkinson[7], and A. Vidal-Madjar[8]
[1] NASA LaRC, Hampton, VA, USA; Guillaume.P.Gronoff@nasa.gov
[2] SSAI, Hampton, VA, USA
[3] BIRA-IASB, Avenue Circulaire 3, 1180 Brussels, Belgium
[4] Aalto University School of Electrical Engineering Department of Radio Science and Engineering, P.O. Box 13000, FI-00076 Aalto, Finland
[5] National Institute of Aerospace, Hampton, VA, USA
[6] IPAG, Grenoble, France
[7] University of Michigan, MI, USA
[8] Observatoire de Paris, Paris, France
Received 2013 September 11; accepted 2014 May 6; published 2014 June 6

ABSTRACT

Characterizing Earth- and Venus-like exoplanets' atmospheres to determine if they are habitable and how they are evolving (e.g., equilibrium or strong erosion) is a challenge. For that endeavor, a key element is the retrieval of the exospheric temperature, which is a marker of some of the processes occurring in the lower layers and controls a large part of the atmospheric escape. We describe a method to determine the exospheric temperature of an O_2- and/or CO_2-rich transiting exoplanet, and we simulate the respective spectra of such a planet in hydrostatic equilibrium and hydrodynamic escape. The observation of hydrodynamically escaping atmospheres in young planets may help constrain and improve our understanding of the evolution of the solar system's terrestrial planets' atmospheres. We use the dependency of the absorption spectra of the O_2 and CO_2 molecules on the temperature to estimate the temperature independently of the total absorption of the planet. Combining two observables (two parts of the UV spectra that have a different temperature dependency) with the model, we are able to determine the thermospheric density profile and temperature. If the slope of the density profile is inconsistent with the temperature, then we infer the hydrodynamic escape. We address the question of the possible biases in the application of the method to future observations, and we show that the flare activity should be cautiously monitored to avoid large biases.

Key words: molecular data – planets and satellites: atmospheres – planets and satellites: detection – ultraviolet: planetary systems

Online-only material: color figures

1. INTRODUCTION

The *CoRot* and *Kepler* missions have observed several Earth-sized exoplanets transiting in front of their stars. The discovery of such planets orbiting in, or near, the habitable zone leads to the question of the existence, the characteristics, and the evolution of the atmospheres around them. Such work is already possible with the atmosphere of hot-Jupiters (Ehrenreich & Désert 2011) and led to the discovery of the evaporation of their atmospheres. The first observations of exoplanetary atmosphere escape were based on the observation of the Lyα line (Vidal-Madjar et al. 2003, 2004), resonant with the corresponding stellar emission. Recently, a stellar light absorption was observed after the transit of a Mercury-sized exoplanet located very close to its star. These observations showed the presence of a comet-like tail which is expected to be formed by the planet's rocky material, which is melting and evaporating because of the extreme hot temperature of this planet ($\approx$2250 K; Brogi et al. 2012).

However, these recent observations concern planets which are likely uninhabitable, at least according to the current definition of habitability (i.e., presence of liquid water on the surface). For Earth- and Venus-sized planets located in the habitable zone, the current challenge is to observe the atmosphere (Ehrenreich et al. 2012). The observation of the evaporation of some Earth-sized atmospheres would be of great importance to understanding the evolution of the terrestrial planets in the solar system and to improve the definition of habitability (Lammer et al. 2013). Indeed, atmospheric erosion is expected to play a significant role for the planet's evolution and can possibly affect the development of life on it as the solar system's telluric planets' case suggests. For example, Venus and Mars are believed to have lost the majority of their atmospheres. Evidence of the presence of large amounts of water flowing on Mars (e.g., Chassefière et al. 2007) contrasts with the small amounts of water that are observed on it now. Similarly, if Venus had the same amount of volatiles as Earth in its atmosphere after its creation and if no significant atmospheric erosion had occurred, its atmosphere would contain much more O_2 and H_2O than what is currently observed. As a consequence, the ground pressure would have been approximately 300 atmospheres instead of the 90 that it is now. The catastrophic greenhouse effect at Venus, followed by the hydrodynamic escape of H and O, is believed to explain the bulk of the Venusian water loss (Kasting & Pollack 1983; Selsis & Halbwachs 2006; Gillmann et al. 2009; Chassefière et al. 2012). However several nonthermal processes may have been as important for the atmospheric escape of the terrestrial planets of the solar system (Tian et al. 2005a, 2005b; Lilensten et al. 2013; Luhmann et al. 2007).

One of the major problems in our understanding of the solar system's planetary atmospheres is our limited knowledge of the evolution of their content with time. Notably, 3–4 Gyr ago, models show that the Sun was fainter, its energy input to Earth's

atmosphere being about 25% lower than today, and therefore liquid water was not sustainable on Earth and Mars without a large greenhouse effect; however, traces of liquid water for these epochs are detected on both planets, and the causes of the greenhouse effect are unclear (Feulner 2012). In this context, the observations of an escaping exoplanetary atmosphere could shed some light on the evolution of the solar system's terrestrial planets' atmospheres.

In order to determine the escape rate of the atmosphere, one of the most important parameters is the exospheric temperature. Knowledge of it allows one to estimate the thermal escape (for nonhydrodynamically escaping) atmospheres and is a key parameter for the other escape processes since it is related to the scale height of the atmosphere. The exospheric temperature can be determined from models when the thermospheric composition is well known. However, minor constituents can have a large influence on that temperature, and therefore direct determination would be preferable. CO_2 is one of the major factors driving the exospheric temperature of a planet: the $CO_2(\nu = 2)$ 15 μm emission is the main cause of the upper atmosphere cooling at Venus, Mars, and Earth. Its efficiency is such that the exospheric temperatures at Venus and Mars, about 200 K, is much lower than those of Earth (800–1600 K) and Jupiter (700–1000 K).

In this paper, we present a technique to determine the exospheric temperature of an exoplanet without the assumption of hydrostatic equilibrium. This technique is based on the temperature dependence of the UV absorption cross-sections of O_2 and CO_2, and is therefore reserved for exoplanetary transits (Section 2). We model the UV spectra of Venus- and Earth-like exoplanets in equilibrium or hydrodynamic escape (Section 3), discuss the uncertainties (Section 4), and show that UV absorption can allow us to discriminate between the two cases, even if the facilities for these observations are not yet available (Section 5).

2. THE MODEL

Planetary atmospheres generally emit in the IR as their temperatures are typically below 1000 K. In addition, the absorption of the thermosphere is negligible in the visible. For example, Vidal-Madjar et al. (2010) show that the altitude range probed by the visible light to extract the temperature in the atmosphere of an exo-Earth is 15–40 km. When considered together, these facts lead to the conclusion that it is advantageous to study thermosphere ($>\approx$100 km at Earth) properties in the UV region of the spectrum.

However, the retrieval of the thermospheric properties from the observation of a transit in the UV implies either a data–model comparison or the determination of the temperature from the resonant stellar line broadening by the atmosphere. The former technique requires an assumption of the escape of the atmosphere, while the latter can be subject to other interpretations, needing careful work to be decisive (Vidal-Madjar et al. 2008). With such work being extremely difficult for telluric planets, we propose to use another approach for the transit's observations in the UV: the dependence of CO_2 and O_2 absorption on the temperature (detailed in Section 2.1). In Figure 2, we show that the O_2 and CO_2 UV spectral absorptions vary with the temperature. Therefore, by observing a planet for which the main absorber is one of these two species, it is possible to infer the mean temperature in the upper atmosphere from the shape of the absorption spectrum.

This technique is the generalization of exoplanetary transits of the method used by Forget et al. (2009) to determine the temperature of the upper atmosphere of Mars. However, in the case of Mars, the planet is known to have a CO_2-rich upper atmosphere, which is not necessarily the case for exoplanets (it depends on the main composition of the atmosphere, the chemical reaction occurring, the photodissociation rate, etc.). Therefore, a necessary first step in the use of the present technique would be the determination of the composition of the atmosphere through the observation of UV emission lines.

To perform the study of the O_2- and CO_2-rich exoplanet transit absorption, we developed a model capable of simulating the absorption spectra of its atmosphere. The objective is to use it as a forward model to interpret future observations. Given an atmosphere model, which consists of the density n_s of each species s and the neutral temperature T as a function of the altitude z, the model computes the absorption cross-section σ for each altitude and wavelength λ through the relation

$$\sigma(z, \lambda) = \sum_s \left(\sigma_s^{\rm tot}(T(z), \lambda) + \sigma_s^{\rm Rayleigh}(\lambda)\right). \quad (1)$$

In addition to the temperature-dependent total absorption cross-sections $\sigma_s^{\rm tot}$ for the species s, Equation (1) uses the Rayleigh scattering cross-section $\sigma_s^{\rm Rayleigh}$ for the given species s.

For the present work, this computation is performed only for a 1D vertical profile, with the assumption of spherical symmetry for the planet's atmosphere, as sketched in Figure 1. The model then computes several lines of sight in the atmosphere, similar to what is done for planetary limb study observations (see Gronoff et al. 2012a). It integrates the absorption profile along these lines to compute the total absorption of the star light along the line of sight. From that, it is possible to perform an integration of the absorption as a function of the radius of the planet (and of the angle if the spherical symmetry is not used) to compute the total absorption by the planet and its atmosphere. If we assume that the parent star has an homogeneous/isotropic emission (the star is described as a homogeneous sphere), the resulting stellar spectrum is computed through the relation

$$E_{\rm surf}(\lambda) = \frac{F(\lambda)}{\pi R^2}, \quad (2)$$

where F is the stellar flux, R the stellar radius, and therefore $E_{\rm surf}$ is the surface flux. It is then possible to compute the observed flux $F_{\rm obs}$ during the transit as the total stellar flux minus the surface flux obscured by the planet in its path and the absorption due to the planet's atmosphere:

$$F_{\rm obs}(\lambda) = F(\lambda) - 2\pi E_{\rm surf}(\lambda)\left(\frac{R_2^2}{2} + \int_{R_2}^{R_3}(1 - e^{-\tau(r,\lambda)})r dr\right). \quad (3)$$

τ is the optical depth of the line of sight passing at the distance r from the center of the exoplanet, computed from $\sigma(z, \lambda)$ by numerical integration for possible coupling with 3D General Circulation Model (GCM) on a spherical grid such as Gitm (Bell et al. 2007; Bougher et al. 2011). R_2 is the planetary radius and R_3 the planetary radius including the atmosphere. In the present case, τ is negligible ($\ll$1) for altitudes greater than 200 km. Without loss of generality, we therefore can consider that R_3 corresponds to the exobase.

Since the main objective is to compute the atmospheric absorption, the stellar flux is not a major parameter as long as its

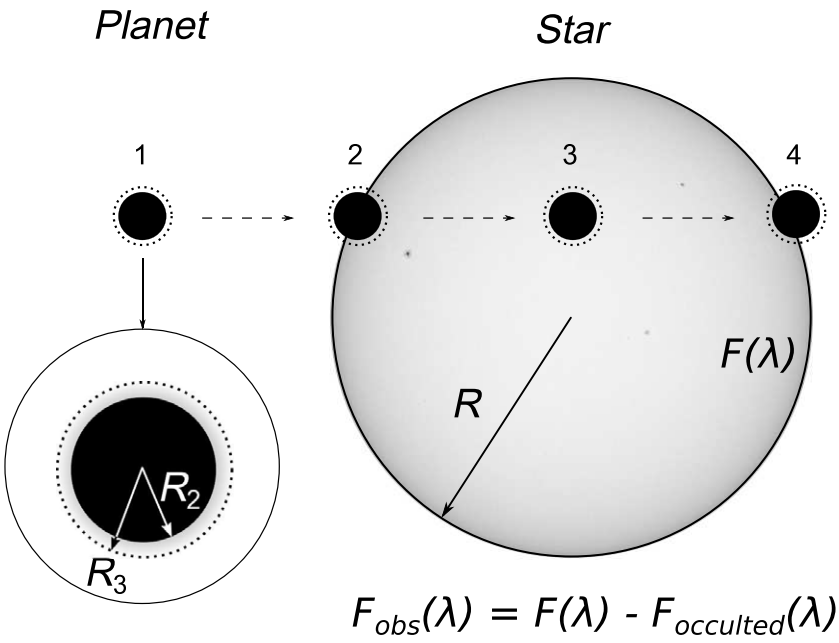

Figure 1. Geometry of a planet transiting in front of its parent star. Four stages are represented: (1) planet outside of the stellar disk, (2) after the first contact, (3) transit, and (4) before the fourth contact. The radius of the planet is R_2, while the height of the atmospheric column measured from the center of the planet is R_3. The star has a radius R and a total unocculted flux $F(\lambda)$. At the time of the transit, the observer sees the contribution of the star flux $F(\lambda)$ minus that which is occulted by the planet $F_{\rm occulted}(\lambda)$.

emissions can be considered as homogeneous and stationary; for transit observations, the star is also observed during nontransit periods to suppress that contribution. The result of a transit observation therefore is the exoplanetary absorption in parts per million (PPM) of the star flux. However, for the observations themselves, a large flux means a better signal-to-noise ratio for the determination of the absorption. In addition, a varying flux may induce biases in the results, which will be analyzed in detail in Section 4.1.1.

The main result of the model, the absorption $A(\lambda)$, is therefore derived from the ratio $F_{\rm obs}/F$ at each wavelength and will be given in PPM in the following. It is computed through

$$A(\lambda) = \frac{1}{R^2}\left(R_2^2 + 2\int_{R_2}^{R_3}(1 - e^{-\tau(r,\lambda)})r.dr\right). \quad (4)$$

For the transit of an exoplanet without atmosphere, the absorption becomes R_2^2/R^2. It means that an exo-Earth would have an absorption of 84 PPM, an exo-Venus 76 PPM, and an exo-Mars 24 PPM. In addition to the radius, the main parameters for our model are the UV absorption cross-sections and the atmosphere model, detailed below.

2.1. The UV Absorption Cross-sections

The computation of the exospheric temperature is based on the temperature dependence of the O_2 and CO_2 cross-sections in the UV and, more precisely, in the 120–200 nm range (Figure 2). The O_2 temperature dependence is due to the Schumann–Runge bands (Minschwaner et al. 1992). The cross-sections have been measured at 90 and 295 K by Yoshino et al. (2005). The CO_2 temperature dependence has been measured by Yoshino et al. (1996) and Stark et al. (2007) at 195 and 295 K (these cross-sections are available at http://www.cfa.harvard.edu/amp/ampdata/cfamols.html). Following Forget et al. (2009), the cross-sections for other temperatures are inferred through linear interpolation and extrapolation. This should be performed very cautiously, especially when very cold temperatures are reached; at Venus, extremely cold temperatures (60 K) have been observed in the mesosphere (Mahieux et al. 2012) very close to the phase transition of CO_2, hence totally modifying the cross-section. For future observations, it will be necessary to measure these cross-sections in a wider range of temperatures.

The UV cross-section for the other species have been compiled in the AtMoCIAD database (Gronoff et al. 2012b), and the cross-sections for Rayleigh scattering have been taken from Sneep & Ubachs (2005).

2.2. The Atmosphere Model

A major input of these simulations is the atmosphere model. The first approach when studying O_2–CO_2-rich exoplanetary atmospheres is to use known atmospheres, especially those of Venus, Earth (Figure 3), or Mars. However, these atmospheres are almost in hydrostatic equilibrium: their escape rate is small, and the mean temperature of the thermosphere is very close to the exospheric temperature.

In Figure 3, we present the thermospheres of Earth and Venus in terms of composition and neutral temperature. The atmosphere of Earth is computed by the MSIS model (Hedin 1991), and the atmosphere of Venus by the VTS-3 model (Hedin et al. 1983; Hedin 1983). At a high altitude, these atmospheres follow an isothermic hydrostatic equilibrium law, meaning that the neutral density for each species follows a law of the form $n_s(z) = n_s(z_{\rm ref}) \times e^{-(z-z_{\rm ref}/H)}$, where H, the scale height, is given by $kT_{\rm prof}/m_s g$; k is Boltzman's constant; m_s is the mass of the species s; and g is the gravitational acceleration at the surface which is be assumed to be constant with the altitude. The profile temperature $T_{\rm prof}$ is the neutral temperature of the atmosphere corresponding to the neutral density law under a hydrostatic equilibrium. It is equal to $T_{\rm exo}$ in the present case, but it is useful for hydrodynamic escape considerations.

The main problem in the model is how to determine the altitude of the mesopause (more accurately the turbopause,

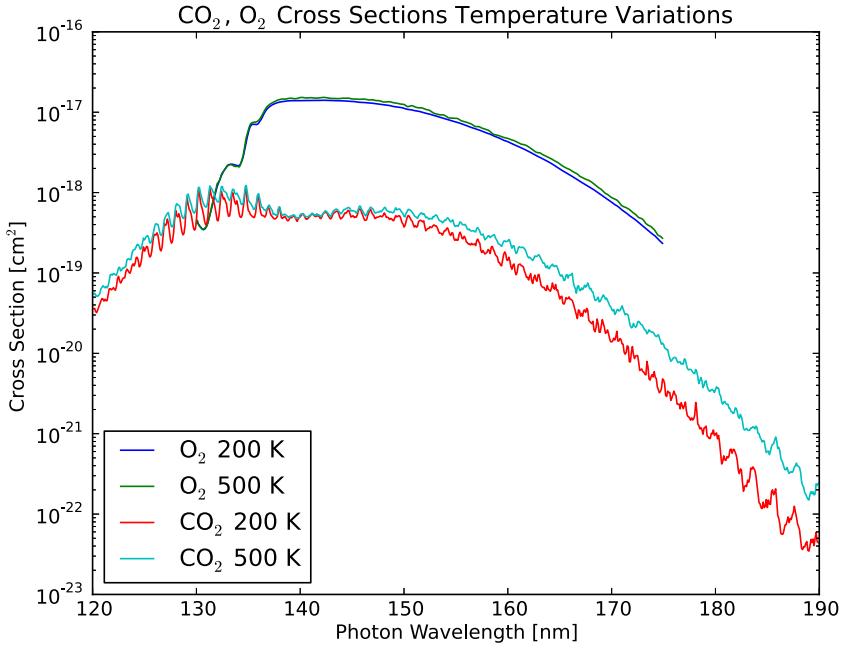

Figure 2. Temperature dependence for the UV absorption cross-sections of O_2 and CO_2.
(A color version of this figure is available in the online journal.)

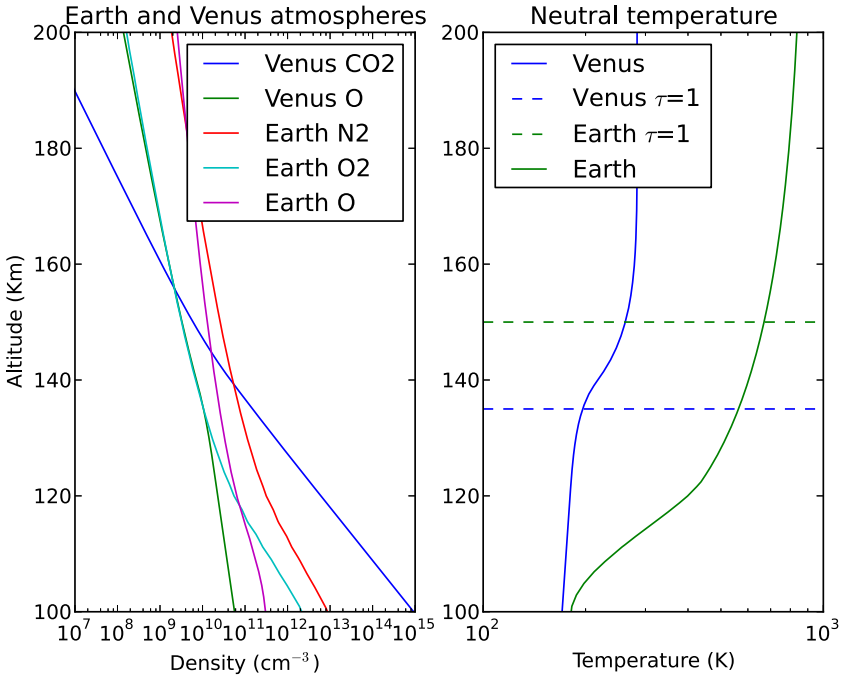

Figure 3. Atmospheres of Earth and Venus. The two atmospheres have different neutral compositions and temperatures in the altitude range considered. The lower temperature of the Venusian thermosphere (sometimes called the cryosphere) is due to the CO_2 15 μm emission cooling. The altitudes for the unit optical depth for the Earth and Venus at 140 nm have been added. The main atmospheric absorption being below that altitude, the transits give little information about the conditions above.

(A color version of this figure is available in the online journal.)

where all species follows their own hydrostatic law), which serves as the reference $z_{\rm ref}$ for the altitudes. The UV flux is totally absorbed below it, so it can be considered as another planetary radius to be accounted for in the determination of the exospheric temperature from the observations. Several solutions exist. (1) Use IR/visible observations, which are more suited for the study of these layers of the atmosphere. (2) Consider the altitude at which the UV flux is totally absorbed at 300 nm to be the reference level. This corresponds to absorption due to the Rayleigh scattering at wavelength for which other processes are negligible, and it is above the mesopause itself, but below altitudes for which $\tau \gg 1$ in the 130–170 nm UV range. (3) Allow the variation in temperature to be dependent on wavelength and use the absorption of several wavelengths in the 130–170 nm UV range. Two points are sufficient to validate the temperature and a third would validate the reference altitude.

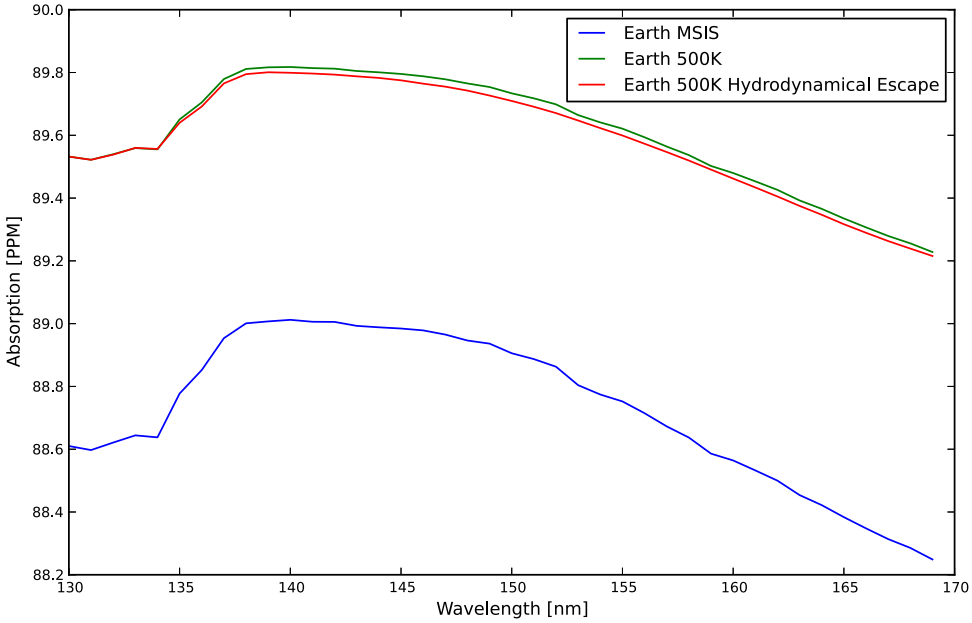

Figure 4. Computation of the absorption spectra for several cases of an extrasolar Earth-like planet.
(A color version of this figure is available in the online journal.)

2.3. Differentiating Hydrostatic Equilibrium and Hydrodynamic Escape

For a hydrodynamically escaping atmosphere, vertical winds are very important, and the vertical density profile is far from that computed from the exospheric temperature and the hydrostatic law. However, the density profile still follows a law close to an exponential. Therefore, it is possible to determine the equivalent of the exospheric temperature to describe that profile. This temperature is the previously defined $T_{\rm prof}$. It means that if we are able to determine the exospheric temperature $T_{\rm exo}$ independently from the total absorption, the simulated absorption from that temperature and the hydrostatic equilibrium hypothesis may be very different from the observation, which gives $T_{\rm prof}$ (in the case of absorption cross-sections independent of T). Therefore, the presented techniques will also be useful to determine if an atmosphere is hydrodynamically escaping. In the following, we will use atmosphere profiles following these exponential laws. However, we will allow $T_{\rm prof}$ to be different from $T_{\rm exo}$; this modification allows a simple comparison of hydrostatic atmospheres with the nonhydrostatic ones, i.e., for which vertical winds exist and the scale height is modified accordingly. We will show that the study of several wavelengths allows de-coupling of the profile and the temperature, allowing the determination of a possible hydrodynamical escape.

3. RESULTS

The model described in Section 2 has been used to compute the UV absorption spectra of Earth and Venus as if they were observed from a very large distance as exoplanets. For these exoplanets, the profile temperature (Section 2.2) and the exospheric temperature have been modified to simulate hydrostatic equilibrium and hydrodynamic escape.

3.1. Temperature Estimation

3.1.1. Earth-like Exoplanets

The transmission spectra of an exo-Earth has been computed by Ehrenreich et al. (2006) for the visible IR region. The UV absorption spectrum for different types of exo-Earths is calculated and presented in Figure 4. The lower curve corresponds to the absorption using the MSIS upper atmospheric model; the upper curve corresponds to an atmosphere in hydrostatic equilibrium, with a $T_{\rm exo} = T_{\rm prof} = 500$ K. The small difference of about 1 PPM between these two curves suggests that the exospheric temperature of the Earth is close to 500 K. However, the actual exospheric temperature of the Earth is higher (700 K). This discrepancy is caused by the fact that the main photoabsorption occurs just above Earth's mesopause (in the 120–150 km region, below altitudes where $\tau = 1$ in Figure 3), where the temperature has not yet reached the exospheric value. This phenomenon prevents the observation of the exact thermospheric temperature, but gives a sufficient constraint on models to retrieve the actual temperature. If a profile temperature of 1000 K had been chosen, the absorption would have been close to 95 PPM. If the profile temperature had been 200 K, the absorption would have been close to 87 PPM, hence a difference of about 8 PPM.

3.1.2. Venus-like Exoplanets

The transmission spectrum of an exo-Venus has been computed in Ehrenreich et al. (2012) for the visible IR region. The UV absorption spectrum for different exo-Venuses is presented in Figure 5. The VTS-3 curve and the 200 K hydrostatic equilibrium curve are almost superimposed, showing that, for the conditions used in the VTS-3 model, the atmosphere of Venus is extremely close to an isothermal hydrostatic equilibrium with an exospheric temperature of 200 K. The temperature variation above altitudes where $\tau = 1$ breaks an assumption in the model, which leads to an incorrect exospheric temperature of 200 K instead of the actual temperature of 300 K. Therefore, more detailed models are needed for accurate retrieval. Both of these curves have an absorption close to 79 PPM along the spectral range. The 1000 K hydrostatic equilibrium profile has many more variations and exhibits a double-hump structure with a first bump at 132 nm corresponding to 85 PPM, a dip at 140 nm/84 PPM, and another bump at 150 nm/84.5 PPM. The absorption goes down on both sides at 190 nm/80 PPM and

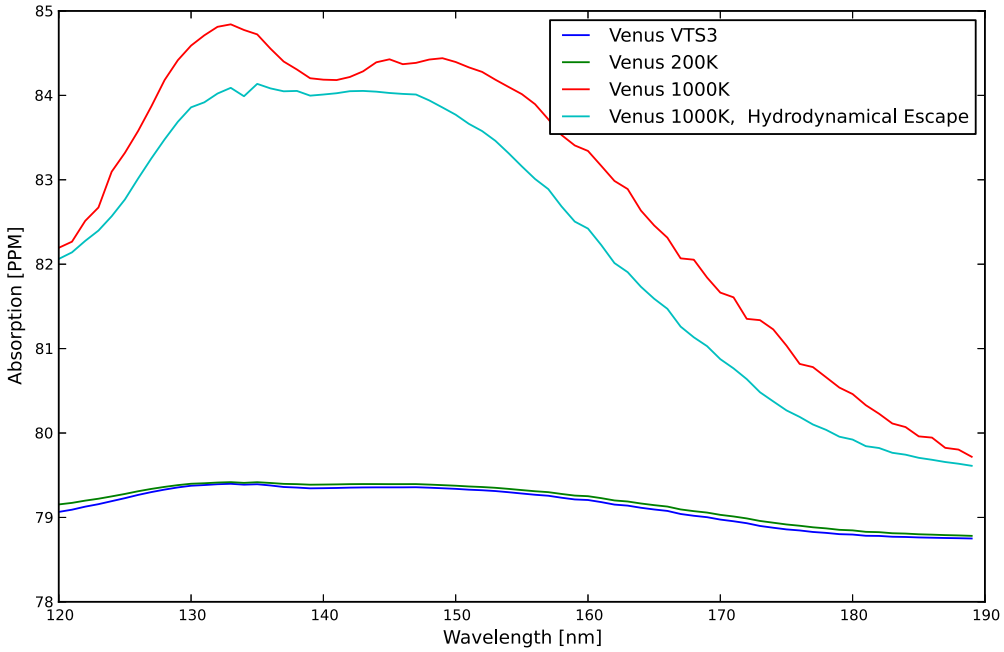

Figure 5. Computation of the absorption spectra for several cases of an extrasolar Venus-like planet.
(A color version of this figure is available in the online journal.)

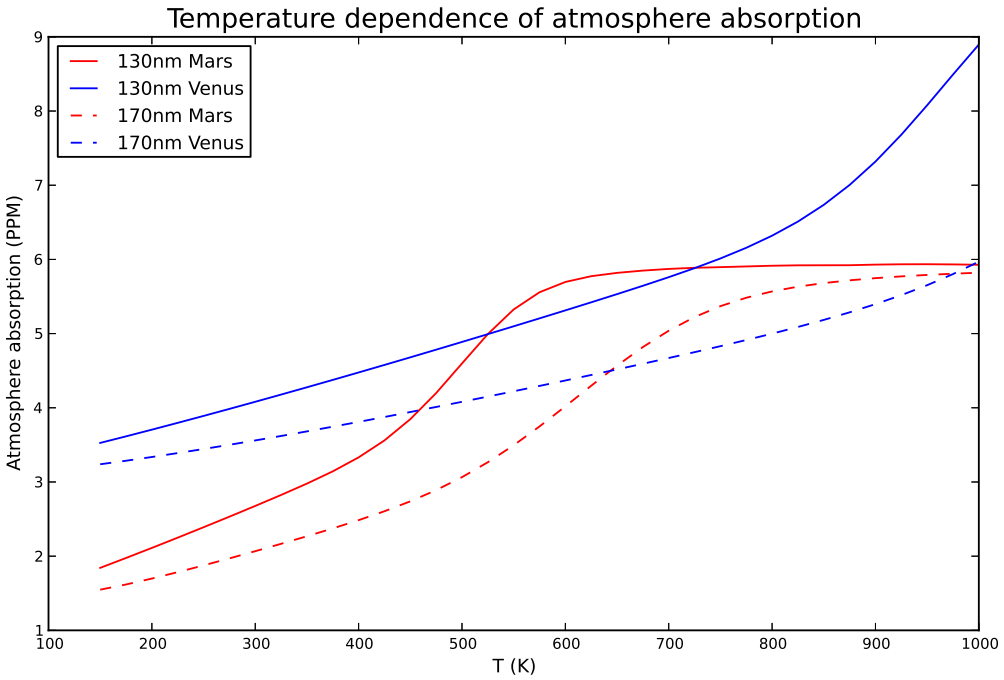

Figure 6. Absorption due uniquely to the atmosphere, as a function of the exospheric temperature, in the case of Mars and Venus in isothermal hydrostatic equilibrium.
(A color version of this figure is available in the online journal.)

120 nm/82 PPM. In addition, a 6 PPM difference calculated between the 200 K and 1000 K curves (79–85 PPM in the 130–150 nm range) is of the same magnitude as the Earth-like case.

Figure 6 represents the absorption at 130 and 170 nm by the atmosphere of Venus and Mars (which can be considered as a Venus-like exoplanets with small radii when dealing with the upper atmosphere) when the term in $(R_2/R)^2$ in Equation (4) was subtracted. The determination of the temperature of an exo-Venus should be done as follows. (1) The figure is created from the determination of the radius of the exoplanet and its composition. (2) The absorptions at 130 and 170 nm are observed. (3) These absorptions are reported on the graph. (4) If the temperatures determined from the two absorptions are equal, then they correspond to the exospheric temperature in the case of an isothermal atmosphere. If the temperatures are in disagreement, it means that if no error in composition and/or radius determination occurred, the planet's atmosphere is in hydrodynamical escape. (5) To improve the determination of the temperature, particularly in the case of a nonisothermal atmosphere, the figure of step (1) could be created from more physical models (e.g., GCM).

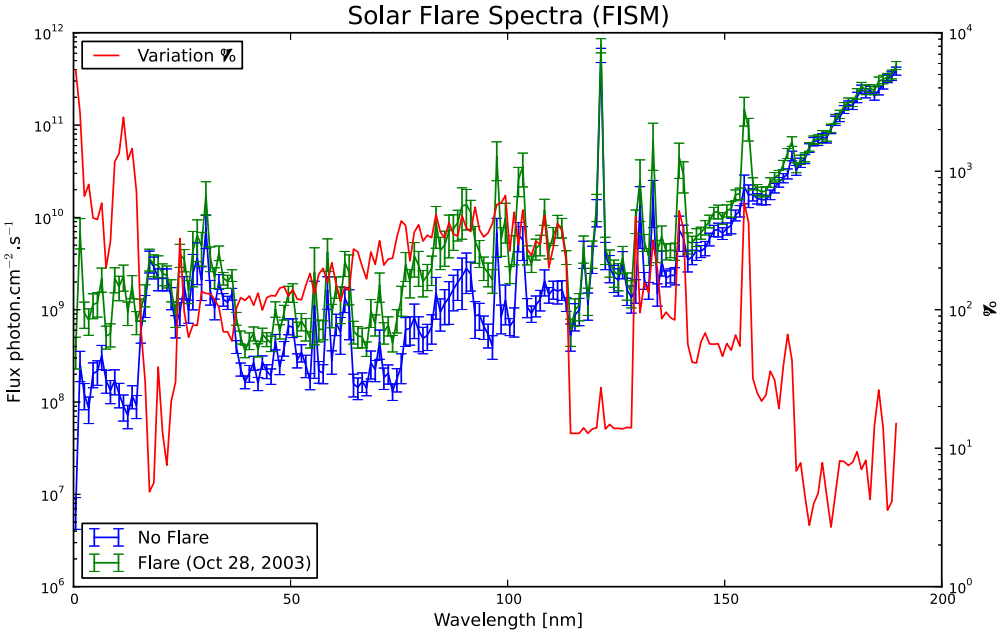

Figure 7. Solar spectra before and during a flare, as modeled by the FISM model (based on observations). Because flares occur on a small portion of their star, an exoplanet crossing that flare may mask it. This could lead to an erroneous interpretation of the state of the planetary atmosphere.

(A color version of this figure is available in the online journal.)

3.2. Hydrostatic Equilibrium versus Hydrodynamic Escape

For the Earth, the comparison between a case of hydrodynamical escape and of hydrostatic equilibrium can be seen in Figure 4. The curve just below the hydrostatic equilibrium curve, labeled "500 K hydrodynamical escape," corresponds to an atmosphere in hydrodynamical escape, simulated with a profile temperature of 500 K, but an exospheric temperature of 200 K. The hydrodynamical escape curve is very close to the 500 K hydrostatic curve, with differences less than 0.05 PPM. Such small differences are due to the relatively small difference in temperature (300 K) between the neutral atmospheres (which have the same temperature profiles) and the small dependence of the absorption with the temperature (Figure 2). If an exo-Earth exists with greater differences between the exospheric temperature and the profile temperature, unfortunately, it is not possible to model them with the correct accuracy since the cross-section in the correct range of temperatures will be needed (for comparison, with the hydrostatic equilibrium at a high temperature).

In contrast, in the case of Venus, the hydrodynamical escape curve of Figure 5, which corresponds to a $T_{\rm prof} = 1000$ K and a $T_{\rm exo} = 200$ K, does not present the double-hump structure of the hydrostatic equilibrium curve and peaks at 84 PPM in the 130–150 PPM range, which creates a 1 PPM peak difference with the 1000 K hydrostatic equilibrium curve. Such a difference is more likely to be detectable in the future. However, the detection of differences in the relative absorption is made difficult by the noise, but also by the different biases that are currently not taken into account in the processing of the data. The sources of uncertainties and biases are listed in the following section.

4. SOURCES OF UNCERTAINTIES

4.1. Sources of Uncertainties/Biases

The main sources of uncertainties, and biases, in the computation of the absorption are as follows.

1. Cross-sections. The different cross-sections used in the model have their relative uncertainties (error in the relative value between two different wavelengths) and inaccuracies (error in the calibration). These uncertainties can be minimized by calibration with an existing source, e.g., by observing Mars (Forget et al. 2009). In addition, it is possible to compute the effect of these uncertainties following a Monte Carlo approach, as described in Gronoff et al. (2012a, 2012b).
2. Stellar spectra (including limb absorption). The stellar emissions are typically not uniform at the surface of the star as supposed in Equation (3). The limb absorption, the presence of flares, or the anomalous redshift of spectral lines due to the sequential eclipsing of one stellar quadrant after the other by the exoplanet, resulting in an observed line broadening (Rossiter–McLaughlin effect; see Ohta et al. 2005) may affect the determination of the absorption coefficient of an exoplanet (Csizmadia et al. 2012). To account for the resulting errors, the star's emissions and its variabilities should be accurately studied (France et al. 2012).
3. Stellar spots/flares. The exoplanet's radius may be non-negligible in comparison with the active regions at the surface of its star. If some active stellar regions are (partially or totally) hidden by the transiting exoplanet, it can be detected as an enhancement or a dip in the stellar flux, which can be misinterpreted as a feature of the exoplanet. An example, using the variability of the solar spectra as determined by the FISM model (Chamberlin et al. 2007, 2008), is shown in Section 4.1.1 and in Figure 7.
4. 3D structure. One of the hypotheses in the model is the spherical symmetry of the atmosphere. More precisely, during the transit, the atmosphere should not vary along the limb of the planet. However, the gravitational waves, the wind structure, etc., and possible comet-like tails (due to large atmospheric escape) may make this assumption invalid. To account more accurately for these effects, it is possible to couple the absorption model with a 3D GCM.

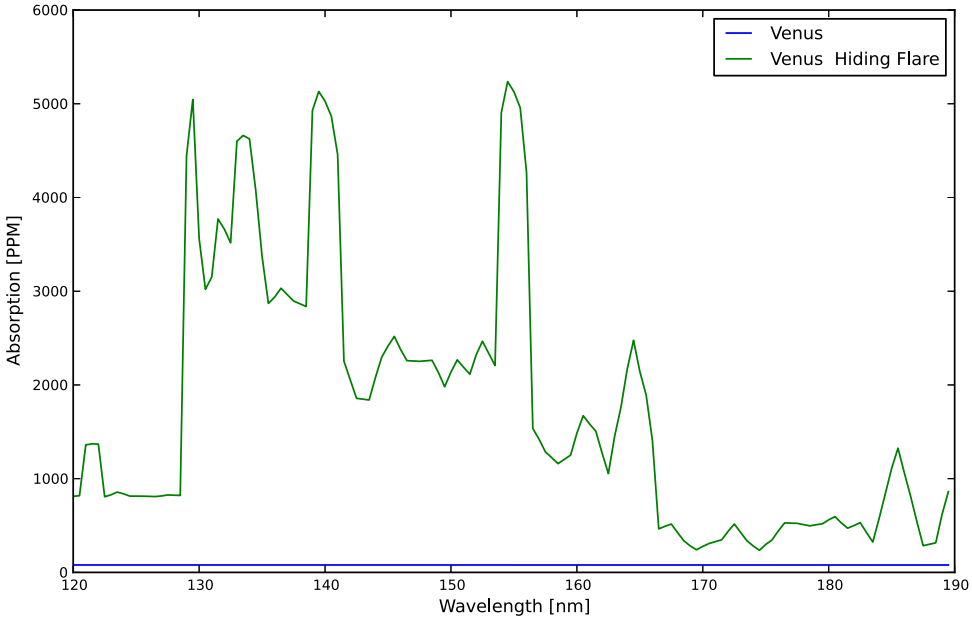

Figure 8. Computation of the actual and the observed absorption of an exo-Venus when a solar flare hiding is not correctly accounted. The flare location masking can artificially create an observed increase in absorption, which can subsequently be falsely interpreted as an increase in the atmospheric size. Such very large effects should be accounted for when studying the small variations in the absorption due to hydrodynamical escape.

(A color version of this figure is available in the online journal.)

5. Nonisothermal state of the upper atmosphere. As seen in Section 3, the temperature retrieved by considering an isothermal atmosphere is not equal to the exospheric temperature because of the neutral temperature variations above the $\tau = 1$ altitude. The consideration of more physical atmospheres, computed with a GCM model, for example, may help solve that problem.
6. Aurora and airglow. UV emissions, similar to Earth's aurora, have also been observed in the nightside of Venus (Fox & Bougher 1991; Gronoff et al. 2008). For giant exoplanets, such emissions have been actively sought (France et al. 2010). However, if we compute the total emitted auroral/airglow power, the effect on the computation of the absorption is several orders of magnitudes below 1 PPM.
7. Radius and mesopause determination. One important parameter in our computation is the knowledge of the radius and the mesopause. Fortunately, by using different wavelengths in the visible and the IR, it is possible to infer the altitude of the mesopause. Indeed, the absorption by Rayleigh scattering above 200 nm is the principal cause of absorption in this spectral region as the atmosphere reaches the optical depth $\tau = 1$ above the mesopause. Using this property, it is then possible to consider the atmosphere only above this limit.

4.1.1. Uncertainty Analysis in the Case of a Solar Flare

The observations of the Venus transit on 2012 June, notably by the *Solar Dynamics Observatory*, showed the planet crossing several bright and dark regions. When an exoplanet crosses its parent star, it may partially or completely mask a solar flare. If the standard procedure for the determination of the absorption is used, the observed flux is divided by the flux of the star. If we suppose that we divide the observation by the flux of the star with the flare when the flare is hidden, the resulting absorption is modified. An example of such an event is shown in Figure 8, along with the absorption that should have been computed. This simulation corresponds to the hypothesis of a Venus-like planet partially hiding the 2003 October 28 flare, whose apparent diameter was assumed to be 25 arcsec for a Venusian diameter of 1 arcsec in that computation. The result of the biased observation is an enhanced (observed) absorption by the planet and can be misinterpreted as an enlargement of the atmosphere. Such effects have large variations with the spectra due to the stellar spectra variations, and therefore can be accounted for. However, since such spectral variations need to be observed for the determination of the exospheric temperature, the determination of a possible exospheric temperature enhancement (Pawlowski & Ridley 2008) during a solar flare should be performed cautiously.

5. DISCUSSION

We demonstrated in Section 3 that both Venus- and Earth-like exoplanets, around a Sun-like star, present a strong dependence of the absorption on the profile temperature, with almost 6 PPM differences between the 200 K and the 1000 K hydrostatic curves at the peak. With the current technology, the small absorption difference prevents the observation of the atmosphere in these conditions, even when the stellar inhomogeneity effects (flares, limb absorption, ...) are correctly taken into account. However, precise computations remain to be performed for most optimal cases, i.e., for an exoplanet relatively larger compared to its star and for more UV-intense stars. Even in these cases, the small difference between the hydrodynamical escape and the hydrostatic equilibrium absorption profiles for the Earth-like exoplanets prevents the determination of the escape by observation only. However, the difference in the spectral absorption structure for CO_2-rich exoplanets give more hope into the possibility of determining whether or not the thermosphere is in equilibrium. Because of the spectral structure (double-hump absorption for equilibrium, single bump for the escaping one), it is even possible to perform that determination without knowing the mesopause altitude (Section 4.1).

For the actual exoplanetary observations, the first (difficult) points before applying the exospheric determination technique

will be to determine the variability and the homogeneity of the parent star emission, the radius of the exoplanet (and the position of the mesopause), and the main composition of the upper atmosphere (to be certain that other species do not contaminate the absorption spectra and, in that case, to perform other absorption simulations to retrieve the correct exospheric temperature). The main factors preventing these observations right now are, in decreasing order of importance, the size and availability of UV telescope, the availability of targets, and the availability of CO_2 and O_2 cross-sections at higher temperatures. It is probable that when the first issue will be solved, the targets will be available as a direct follow-up. Updating the cross-sections is a work in progress (Venot et al. 2013).

For the study of atmospheric and climate evolutions, an interesting target will be the young stellar systems. The observation of a hydrodynamically escaping Venusian or Martian atmosphere could help understand the history of CO_2-rich planetary atmospheres in our solar system.

6. CONCLUSION

This paper presents a new technique to determine the exospheric temperature of CO_2- and O_2-rich transiting exoplanets, along with a tool allowing the determination of whether or not a CO_2-rich atmosphere is hydrodynamically escaping. The technique is based on the use of the CO_2 and O_2 UV cross-section dependence on the neutral temperature, following a technique already applied at Mars. The determination of the exospheric temperature and of the hydrodynamic/hydrostatic state of an atmosphere is necessary to understand its evolution. The observation of young Venus- and Earth-like exoplanets may help understand the variability of the atmospheres in our own solar system, as well as their evolution. Such observations will be a challenge for the next generation of the space-based UV telescope, requiring optimal conditions for the observation, but could bring new insight on the fate of planetary atmospheres.

We are grateful to A. Lecavelier (IAP, Fr), D. Ehrenreich (Univ. Geneva, CH), J. Lilensten, M. Barthelemy (IPAG, Fr), and A. Gopalan (SSAI/NASA LaRC, USA) for useful discussions.

REFERENCES

Bell, J. M., Bougher, S. W., & Murphy, J. R. 2007, JGRE, 112, 12002
Bougher, S. W., Ridley, A., Pawlowski, D., Bell, J. M., & Nelli, S. 2011, in Mars Atmosphere Conference, Mars Atmosphere: Modelling and Observation, ed. F. Forget & E. Millour, 379
Brogi, M., Keller, C. U., de Juan Ovelar, M., et al. 2012, A&A, 545, L5
Chamberlin, P. C., Woods, T. N., & Eparvier, F. G. 2007, SpWea, 5, S07005
Chamberlin, P. C., Woods, T. N., & Eparvier, F. G. 2008, SpWea, 6, S05001
Chassefière, E., Leblanc, F., & Langlais, B. 2007, P&SS, 55, 343
Chassefière, E., Wieler, R., Marty, B., & Leblanc, F. 2012, P&SS, 6364, 15
Csizmadia, S., Pasternacki, T., Dreyer, C., et al. 2012, A&A, 549, A9
Ehrenreich, D., & Désert, J.-M. 2011, A&A, 529, A136
Ehrenreich, D., Tinetti, G., Lecavelier Des Etangs, A., Vidal-Madjar, A., & Selsis, F. 2006, A&A, 448, 379
Ehrenreich, D., Vidal-Madjar, A., Widemann, T., et al. 2012, A&A, 537, 6
Feulner, G. 2012, RvGeo, 50, RG2006
Forget, F., Montmessin, F., Bertaux, J.-L., et al. 2009, JGR, 114, E1
Fox, J. L., & Bougher, S. W. 1991, SSRv., 55, 357
France, K., Linsky, J. L., Tian, F., Froning, C. S., & Roberge, A. 2012, ApJL, 750, L32
France, K., Stocke, J. T., Yang, H., et al. 2010, ApJ, 712, 1277
Gillmann, C., Chassefière, E., & Lognonné, P. 2009, E&PSL, 286, 503
Gronoff, G., Lilensten, J., Simon, C., et al. 2008, A&A, 482, 1015
Gronoff, G., Wedlund, C. S., Mertens, C. J., et al. 2012a, JGR, 117, 17
Gronoff, G., Wedlund, C. S., Mertens, C. J., & Lillis, R. J. 2012b, JGR, 117, 18
Hedin, A. E. 1983, JGR, 88, 6352
Hedin, A. E. 1991, JGR, 96, 1159
Hedin, A. E., Niemann, H. B., Kasprzak, W. T., & Seiff, A. 1983, JGR, 88, 73
Kasting, J. F., & Pollack, J. B. 1983, Icar, 53, 479
Lammer, H., Erkaev, N. V., Odert, P., et al. 2013, MNRAS, 430, 1247
Lilensten, J., Simon Wedlund, C., Barthélémy, M., et al. 2013, Icar, 222, 169
Luhmann, J. G., Kasprzak, W. T., & Russell, C. T. 2007, JGR, 112, E04S10
Mahieux, A., Vandaele, A. C., Robert, S., et al. 2012, JGR, 117, E07001
Minschwaner, K., Anderson, G. P., Hall, L. A., & Yoshino, K. 1992, JGR, 97, 10103
Ohta, Y., Taruya, A., & Suto, Y. 2005, ApJ, 622, 1118
Pawlowski, D. J., & Ridley, A. J. 2008, JGRA, 113, 10309
Selsis, F., & Halbwachs, J.-L. 2006, in Formation planétaire et exoplanètes, Ecole thématique du CNRS, Goutelas (Loire), 2005 May 23–27, ed. J.-L. Halbwachs, D. Egret, & J.-M. Hameury (Strasbourg: Observatoire astronomique de Strasbourg et Société Franaise d'Astronomie et d'Astrophysique (SF2A)), 271
Sneep, M., & Ubachs, W. 2005, JQSRT, 92, 293
Stark, G., Yoshino, K., Smith, P., & Ito, K. 2007, JQSRT, 103, 67
Tian, F., Toon, O. B., Pavlov, A. A., & De Sterck, H. 2005a, ApJ, 621, 1049
Tian, F., Toon, O. B., Pavlov, A. A., & De Sterck, H. 2005b, Sci, 308, 1014
Venot, O., Fray, N., Bénilan, Y., et al. 2013, A&A, 551, A131
Vidal-Madjar, A., Arnold, L., Ehrenreich, D., et al. 2010, A&A, 523, 57
Vidal-Madjar, A., Dsert, J.-M., Etangs, A. L. d., et al. 2004, ApJL, 604, L69
Vidal-Madjar, A., Etangs, A. L. d., Désert, J.-M., et al. 2003, Natur, 422, 143
Vidal-Madjar, A., Lecavelier des Etangs, A., Désert, J.-M., et al. 2008, ApJL, 676, L57
Yoshino, K., Esmond, J., Sun, Y., et al. 1996, JQSRT, 55, 53
Yoshino, K., Parkinson, W., Ito, K., & Matsui, T. 2005, JMoSp, 229, 238